Advances in Nanochemistry

Article

The effect of solvent and temperature on the optical and structural properties of the nickel oxide and Cu-doped nickel oxide nanoparticles

Received 26th October 2018,
Accepted 14th Novomber 2018,
DOI:

Khalilollah Sayyadi[1], Mahsa Gharani[2,*], Abbas Rahdar[3]

[1] Young Researchers Society, Shahid Bahonar University of Kerman, Department of Chemistry, Kerman, 7619, Iran
[2] Departments of Solid-state Physics, universty of Sistan and Baluchestan , Zahedan, Iran
[3] Departments of Physics, Faculty of Science, University of Zabol, Zabol, Iran

Abstract

In the current work, nickel oxide (NiO) and copper-doped nickel oxide (Cu-NiO) nanoparticles were prepared by co-precipitation method. The effect of Cu doping on the structural and optical features of NiO nanoparticles and the effect of solvent and temperature on the optical and structural properties of nickel oxide and Cu-doped nickel oxide nanoparticles were studided by X-ray diffraction (XRD), ultraviolet-visible (UV-Vis) spectroscopy, fourier transform-infrared (FT-IR) spectroscopy and vibrating-sample magnetometer (VSM) technique. The XRD analysis condirmed that the Cu-doped nickel oxide have a cubical structure and showed that the crystalline size increased with the increase of temperature. The optical absorption spectra of the structures illusterated a blue-shift with decreasing in crystal size so that the energy gap of nickel oxide decreased with increasing temperature. Subsequently, in the presence of propranol and without ethylene glycol, the Cu-doped NiO band gap was the lowest and with the applying of ethanol and ethylene glycol was the highest amount. Magnetization property study of the nanoparticles performed at room temperature confirmed the weak ferromagnetic behavior of Cu-doped NiO nanoparticles before calcinations. The magnetization in the magnetic hysteresis loop indicated that nanoparticles have super paramagnetic property after calcination.

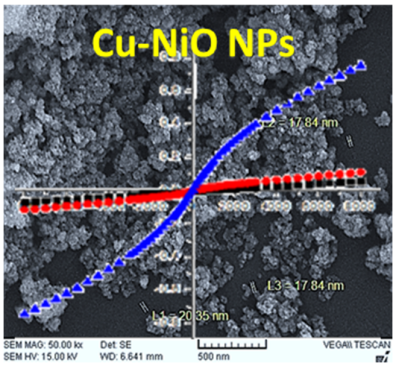

***Keywords*:** *Cu-doped nickel oxide, Co-precipitation, VSM, Optical band gap, XRD.*

Introduction

Over the past 30 years, metallic oxide nanostructures (MONs) of 1 to 100 nm have been pursued intensively for their fundamental scientific advances and their numerous applications such as photocatalyst, sensor, adsorption, solar cell and medicine.[1-6] MONs have suitable magnetic, optical, electrical and chemical properties,[7, 8] which depend to their size, so that these features will be noticeable by reducing their size.[1] Among the wide range of MONs, nickel oxide has attracted the interest of many researchers. Nickel oxide is a P-type semiconductor and powder of a green colour that acts as a receiver of electrons.[9] This semiconductor, has an energy band width of 3.4 ev to 4 ev, a robust band gap and a large optic in the area of the visible.[10] Typically, reducing the size of the nickel oxide semiconductor causes a significant decrease in the width of the valance and the conductivity bands, which leads to an enhance in the energy gap.[11] This material has the potential to be used in catalysts,[12] cathodic batteries,[13] gas sensors,[14] electrochemical films,[15] magnetic materials for active optical fibers,[16] fuel cells,[16] smart windows,[18] capacitors,[19] and composites.[20] Several physical and chemical ways for the manufacturing of nickel oxide have been developed. Physical procedures such as electrodeposition and ball milling have high purity advantages and ease of ability production of this metal oxide.[21-23] However, controlling the size and supplying particles of the same size with physical methods is very difficult. Therefore, chemical methods are suggested to counteract this problem.[24] The chemical processes are based liquid phase of coloidical chemistry[25] and include routes as co-precipitation,[26] surfactants-mediated,[27] thermal decomposition[28] and other techniques. Herein, we have utilized the co-precipitation method to synthesize Cu dopes NiO. Finally, the effects of doping on optical, electrical and magnetic properties of nickel oxide were investigated.

Experimental

Materials and methods

$Ni(NO_3)_2$, $Cu(NO_3)_2$ and NaOH were purchased from Merck and Aldrich, and used without further purification. The X-ray diffraction experiment (XRD belonging to Rigaku-Miniflex model) was recorded using Cu Kα radiation (λ= 0.1541 nm). FT-IR spectra were obtained with the JASCO 640 plus infrared spectrometer in the range of 400-4000 cm^{-1} using the KBr disk technique. The vibrating sample magnetometer (VSM) device, in the Development Center of University of Kashan (Kashan, Iran). The absorption was measured using a USB-2000 UV–Vis spectrophotometer.

Corresponding author: Mahsa Gharani
Email: m.a.h.gharani@gmail.com

Synthesis of NiO nanoparticle

To prepare NiO nanoparticles by co-precipitation method, 2.32 g of $Ni(NO_3)_2$ was dispersed in the solvent and after 60 min of stirring, a certain of NaOH was added to the solution to increase the precipitate. Thereafter, the solution was centrifuged and washed with distilled water. In finally step, the collected solid dried at 100 °C for 14 hr. Subsequently, the obtained product was calcinated in 500 °C and 700 °C and afford the final of black powder.

Synthesis of Cu doped NiO nanoparticle

First, the certain amount of $NiCl_2.6H_2O$ and $CuCl_2.2H_2O$ were dissolved in double-distilled water as solvent to get a certain molar concentration with a molar ratio of X=Cu/(Cu+Ni)=0.13 at room temperature. Then, obtained solution was stirred for 40 min at 50 °C. After that, 0.1 M NaOH solution was added slowly, centrifuged and the resulting sample was dried at 100 °C for 14 hr. In the fallowing, the dried product was calcinated at 500 °C and 700 °C to reach Cu - doped NiO.

Synthesis of NiO nanoparticle and Cu-doped NiO nanoparticle by using ethylene glycol as surfactant

The production of NiO nanoparticle and Cu-doped NiO using surfactant as previously described, but in this step 10 ml ethylene glycol was added at the end of the reaction to the solution. After adding surfactant, the solution was stirred for 15 minutes.

Results and discussion

XRD analysis

The XRD analysis of Cu-doped NiO structure is shown in Figure 1a at different temperatures. As shown in Figure 1a, at calcine temperature of 500 °C the peaks at 2θ values of 29°, 35°, 37°, 38°, 43°, 48°, 62°, 66° and 68° were respectively correspond to the (110), (211), (111), (200), (20-2), (220), (310) and (22-1) planes. As seen in Figure 1b, at calcine temperature of 700 °C the peaks observed in the 2θ angles of 35°, 37°, 38.64°, 38°, 43°, 48°, 53°, 58°, 61°, 62°, 63°, 66° and 68° related to (211), (111), (200), (200), (202), (020), (224), (11-3), (220), (310) and (22-1) reflections planes. Figure 1a and b discloses that for Cu-doped NiO nanoparticles with an increase in temperature from 500 °C to 700 °C, the average size of nanoparticles, peak intensity and crystallinity enhanced. The average crystallite size (D) of structures were calculated using the Scherer formula using (111) plane reflection from the XRD pattern as follows:

$$D_{h,k,l}=0.9\lambda/(\beta_{h,k,l}\cos\theta) \quad (1)$$

Where λ is the wavelength (λ = 1.542 Å) (CuKα), β is the full width at half maximum (FWHM) of the line, and θ is the diffraction angle. From the Scherrer equation the average crystalline size of Cu-doped NiO nanoparticle at 500 °C is 49 nm while at 700 °C is 55 nm. The XRD patterns of Cu-doped NiO in in presence (Figure 1c) and absence (Figure 1d) of ethylene glycol Figure 1d) at 500 °C is revealed. According to Figure1c, the peaks are obtained at 2Θ = 35°, 37°, 38°, 43°, 48°, 62°, 65° and 68°, which are dedicated to (211), (111), (200), (200), (20 – 2), (220), (310) and (221) planes, respectively. Also, the peaks observed in the 2θ angles of 29, 35, 37, 38, 43, 48, 62, 66, and 68 are referred to (110), (211), (111), (200), (200), (202), (220), (310) and (221) plane reflections (Figure 1d). Due to, XRD of pattern related to the presence of ethylene glycol in comparison to without of ethylene glycol sample, peak width increased and the average crystallite size when the ethylene glycol is 47 nm and in the absence of ethylene glycol is reported 49 nm.

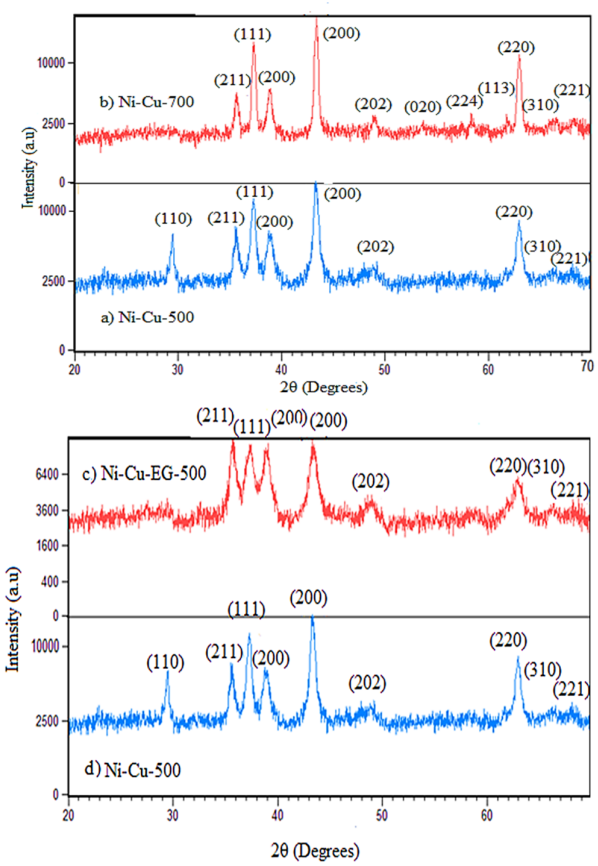

Figure 1. *a) The XRD pattern of Cu doped NiO nanoparticle (500°C), b) The XRD pattern of Cu doped NiO nanoparticle (700°C), c) The XRD pattern of Cu-doped NiO nanoparticle (with ethylene glycol) and d) The XRD pattern of Cu-doped NiO nanoparticle (without of ethylene glycol).*

The vibrating-sample magnetometer analysis

Figure 2 shows the hysteresis curve of pure NiO nanoparticles at diverse temperatures (300, 500, and 700° C). As the calcination temperature raised up, the super-paramagnetic state curve becomes an anti-ferromagnetic state, because with increasing calcination temperature, the particle size and surface-to-volume ratio was decreased. Also, enhancing the temperature will rise the thermal imbalance and reduce the magnetism. Consequently, with increasing temperature, the magnetic saturation (Ms) reduces, and the superparamagnetic, in which single-domain particles are in the anti-ferromagnetic behaviour, are changed, where the momentum of the magnetic atoms is oriented in a combination of parallel, and the curve changes being linear.[29] The results of the VSM analysis for NiO nanoparticles are summarized in Table 1, where with increasing calcination temperature and particle size in a constant saturation field (Oe), the Ms is decreased.

Table 1. *The outcomes obtained from the VSM analysis at 300, 500 and 700 °C.*

Sample	Magnetic saturation (m_s) (emu/g)	b_s Saturation field (o_e)
NiO-300	0.74913	8000
NiO-500	0.11076	8000
NiO-700	0.05729	8000

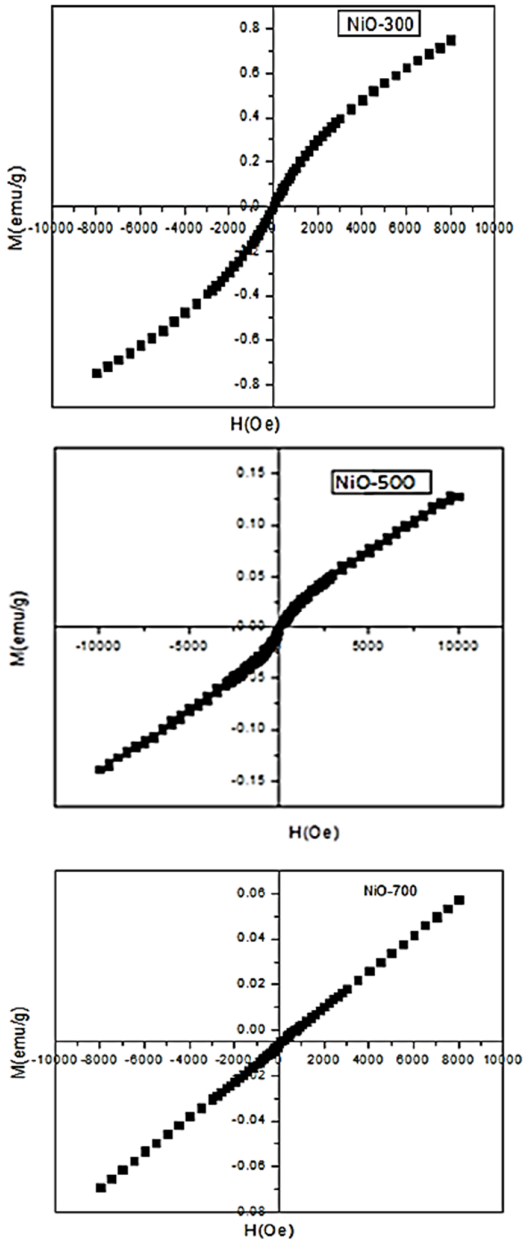

Figure 2. *The magnetic hysteresis curve of pure NiO nanoparticles at different calcination temperatures 300, 500 and 700°C*

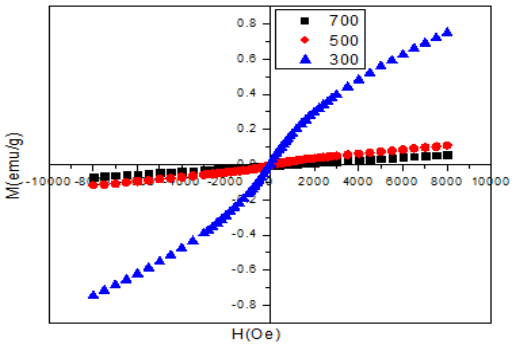

Figure 3. *The magnetic hysteresis curves of NiO nanoparticle at 300, 500, and 700 °C.*

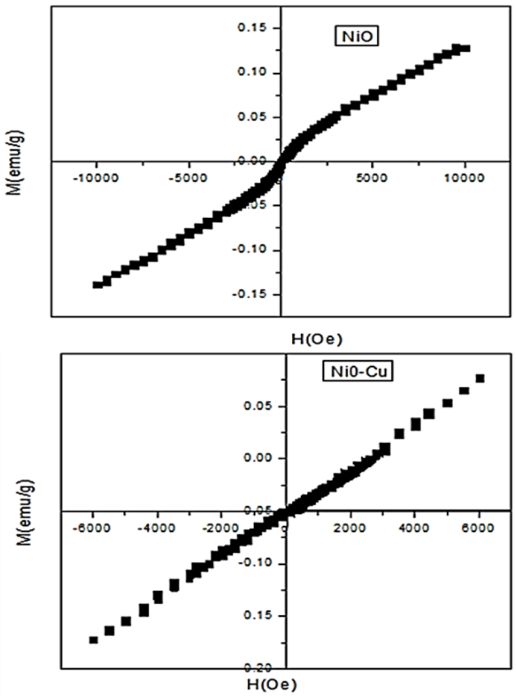

Figure 4. *The magnetic hysteresis curve of NiO and Cu-doped NiOnanoparticles.*

The NiO nanoparticles magnetic hysteresis hybrid curve in different calcining temperatures was investigated and the corresponding esults are shown in Figure 3. The results indicates a curvature in the central region of the diagram. In lower temperatuers the curve is linearized, since the Ms is declined with rising temperature and increasing particle size. Figure 4 shows a comparison between the magnetic hysteresis curve of NiO and Cu-doped NiO nanoparticles. As seen, the amount of Ms is 0.0711 in the Oe = 6000 and emphasizes that Cu-doped NiO nanoparticles are anti-ferromagnetic.

The FT-IR spectroscopy

The FT-IR spectrum is devoted to pure nickel in Figure 5a. The broad absorption bands at 3445.8 cm^{-1} and 2362.93 cm^{-1} belong to the O-H and CO_2 groups, respectively. The absorption band at 1632.44 cm^{-1} was due to the O-H bond, which is resulted from the presence of water in the sample.[31] A characteristic peak at 1420.53 cm^{-1} related to the CO_3^{2-} and a band at 1171.07 cm^{-1} is due to the adsorbed air molecule. The absorption bands of Ni-O observed at 522.67 cm^{-1} and 470.56 cm^{-1} that represents the formation of NiO molecules and the absorption band at 619.3 cm^{-1} is correspond to the Ni-O-H bond.[32] In Figure 5b, the FT-IR spectrum of NiO nanoparticles at 300 °C shows the absorption peak of O-H indicated at 3448.97 cm^{-1}. The absorption band at 3262.96 cm^{-1} is related to the CO_2 bond. The absorptions 1383.17 cm^{-1} and 1400 cm^{-1} confirm the CO_3^{2-} bonds.[32,33] Moreover, three absorption bands at 533.97 cm^{-1}, 466.61 cm^{-1} and 443.83 cm^{-1} respectively are dedicated to the Ni-O group. Subsequently, Ni-O-H group is belong to the typical peak in at 636.40 cm^{-1}. The FT-IR spectrum of the NiO nanoparticle at 700 °C has been investigated in Figure 5c. The O-H bond is revealed to the 3383.38 cm^{-1} and the absorption band at 2921.07 cm^{-1} is due to the C-H group. The peaks of 514.93 cm^{-1} and 469.62 cm^{-1} are ascribed to the Ni-O bond in the sample.[33-35] The FT-IR of Cu-doped NiO is evaluated at 500 °C in Figure 5d. Given to this spectrum, the bands of 2428.12 cm^{-1} and 2362.87 cm^{-1} is

relevant to CO_2 molecules.[36] The peak emerged at 3420.32 cm^{-1} is assigned to O-H bond. The absorption peaks at 1632.59 cm^{-1} correspond to the O-H bonds presence in the sample and the CO_3^{2-} peak is in the region of 1382.44 cm^{-1}.[32]

Characteristics of NiO are placed at *ca*.515.44 cm^{-1}, 461.67 cm^{-1} and 441.30 cm^{-1}. The C-O group caused an absorption band at 833.36 cm^{-1}. The band attributed to the Cu-O group is observed at 833.36 cm^{-1}.[32] Two absorption peaks at 484.77 cm^{-1} and 449.98 cm^{-1} in the FT-IR spectrum at a temperature of 700 °C is suggested for Ni-O bond[33] in Figure 5e. The Cu-O group is confirmed at 415.12 cm^{-1}.[34, 35] In this spectrum, the O-H of bonds do not exist because the Cu-doped NiO sample is calcined at 700 °C. The optical specifications of the prepared samples and the effect of solvent on the optical properties were also confirmed by the use of the UV-Vis spectroscopy.

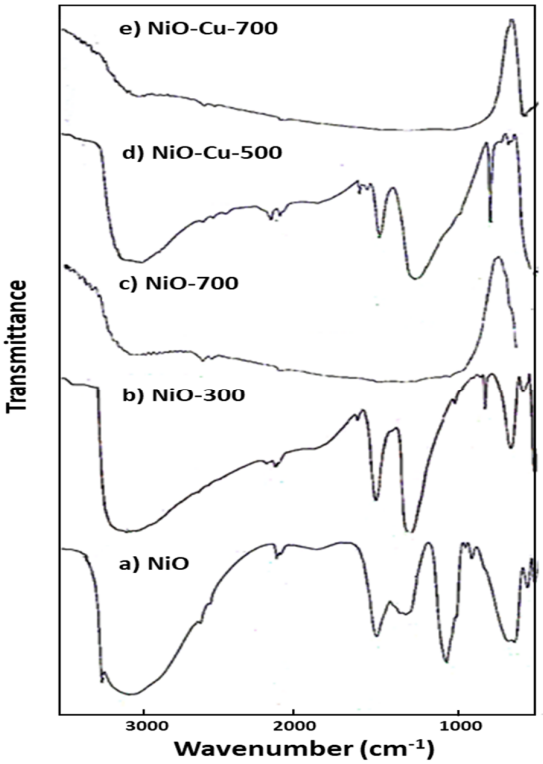

Figure 5. *The FT-IR spectra of a) NiO, b) NiO-300, c) NiO-700, d) NiO-Cu-500 and e) NiO-Cu-700 samples.*

Optical characterization

The UV-Vis spectra of the pure NiO at 300, 500, and 700 °C are demonstrated in Figure 6. The absorption edge is indicated in the range of 280-350 nm which has decreased by the calcination temperature. The absorption edge was also shifted toward the blue wavelengths. The obtained direct optical band gap values for samples are shown in Table 2. It is necessary to mention that the optical direct band gap values of the samples were determined by Tauc's relation:[33]

$$\alpha h\upsilon = \alpha_0 (h\upsilon - E_g)^{1/2} \quad (2)$$

Where hν, α_o and E_g are photon energy, a constant and optical band gap, respectively. The absorption coefficient (α) of the samples can be determined from the absorption spectra at different wavelengths. The values of E_g were calculated by extrapolations of the linear regions of the plot of $(\alpha h\nu)^2$ versus ħν.

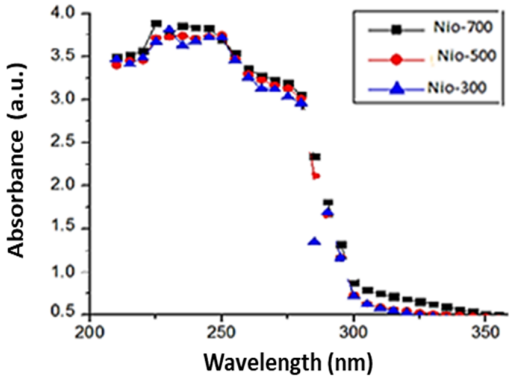

Figure 6. *Measuring the energy gap of pure nickel oxide at calcination temperatures 300, 500, and 700 °C by their absorption spectra.*

Table 2. *The band gap related to pure nickel oxide samples at different calcination temperatures.*

Calcination temperature (°C)	300	500	700
Energy gap (eV)	4	3.90	3.80

Table 3. *The band gap for a sample of NiO and Cu-doped NiO nanoparticles.*

Sample	NiO	NiO-Cu
Energy gap (eV)	3.90	3.92

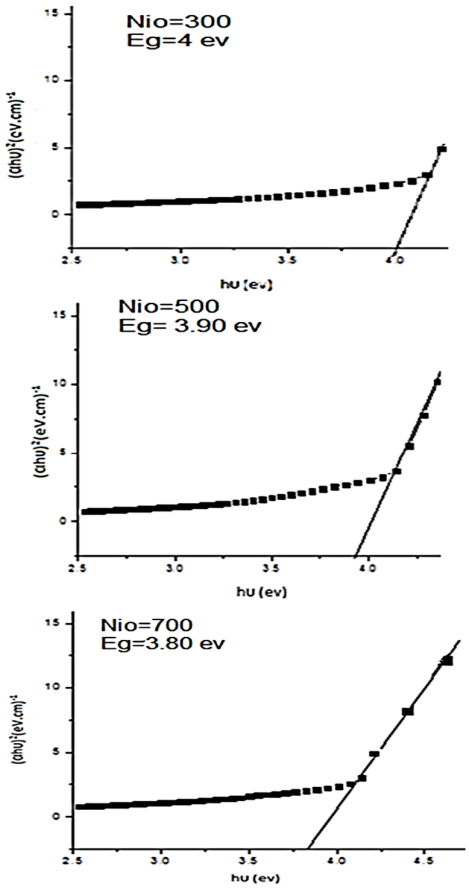

Figure 7. *The determination of energy gap of NiO and Cu- doped NiO by their absorption spectra.*

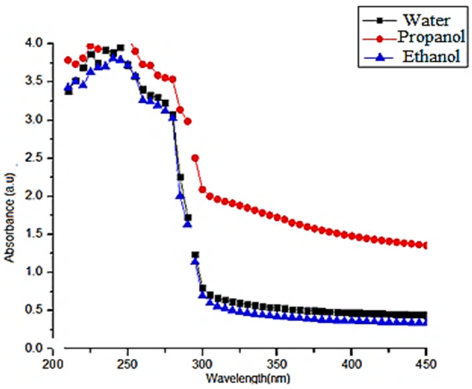

Figure 8. *The absorption spectra of Cu-doped NiO nanoparticle in diverse solvents.*

As shown in Table 2, upon enhancing calcination temperature, the particle size increased and the band gap energy width has diminished. The optical properties of NiO and Cu-doped NiO nanoparticles are shown in Figure 7. The optical band gap values increased with the increase of doping concentration. The calculated data for the energy gap is summarized in Table 3 which is in accordance with relation (2).

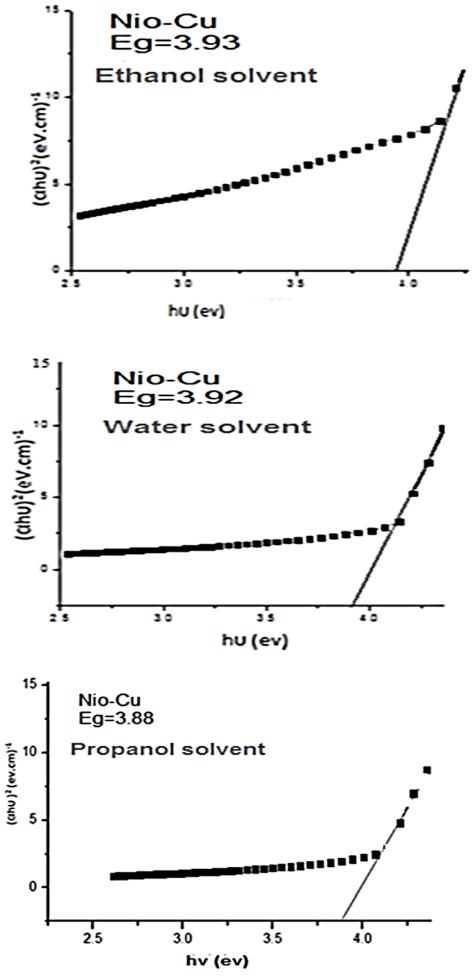

Figure 9. *Representing the evaluated energy gap of Cu-doped NiO nanopaticle in various solvents by their absorption spectra.*

The effect of solvent on optical properties

The ultra UV-Vis spectroscopy results from the effects of propanol, ethanol, and water solvents on Cu-doped NiO nanoparticle, show a shift towards the blue wavelengths as a result of a decrease in size, while all conditions except solvents are the same (Figure 8). This plot was in accordance with the calculated band gaps 3.93, 3.92 and 3.88 eV for Cu-doped NiO samples in different solvents including ethanol, water and propanol, respectively (Figure 9).

Figure 10 demonstrates comparison of the absorption spectra of nickel oxide nanoparticles in the presence and absence of ethylene glycol. By adding ethylene glycol, the absorption edge revealed a blue-shift, indicating smaller size and larger energy gap. In other words, the samples exhibit a wide range of optical transparency.

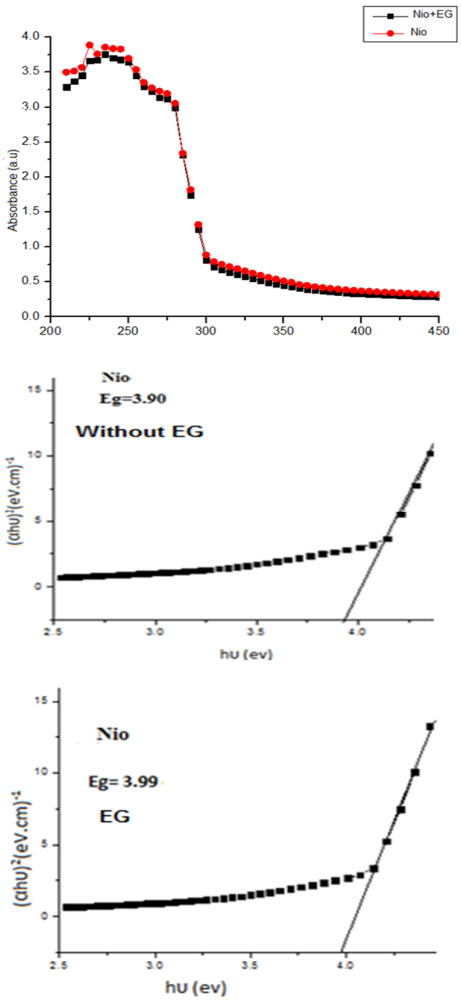

Figure 10. *Upper plot shows the absorption spectra of NiO nanoparticles in the absence and presence of ethylene glycol. Below illustrate determination of the NiO nanoparticles energy gap in the presence and absence of ethylene glycol, using their absorption spectra.*

In Figure 10, the band gap of NiO nanoparticles in the presence and absence of ethylene glycol was respectively evaluated as Eg = 3.99 eV and Eg = 3.90 eV which proves the effect of ethylene glycol on

the particle size reduction. Like NiO nanoparticle absorption spectrum, Cu-doped NiO nanoparticles absorption spectrum displays a shift towards the blue wavelengths, and the bandwidth in the presence and absence of ethylene glycol was calculated as Eg = 4 and Eg = 3.92 , respectively (Figure 11).

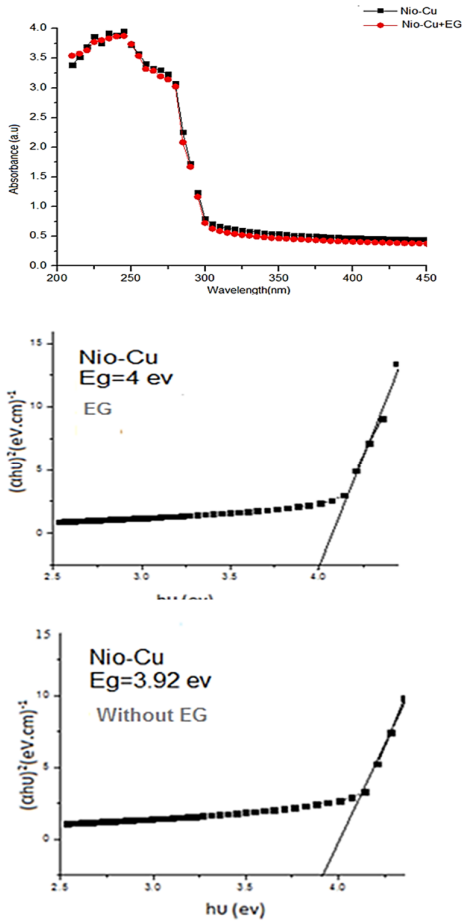

Figure 11. *Upper plot shows the absorption spectra of NiO nanoparticles in the absence and presence of ethylene glycol. Below illustrate determination of the NiO nanoparticles energy gap in the presence and absence of ethylene glycol, using their absorption spectra.*

Figure 12 shows the scanning electron microscopy (SEM) image of Cu-doped NiO nanoparticles (X=0.13). It is clear that the nanoparticles are nearly spherical**.**

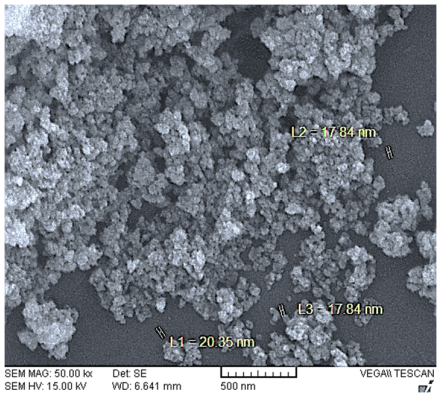

Figure 12. *The SEM image of Cu-doped NiO nanoparticles*

Conclusion

In this paper, we have described a simple procedure for the synthesis of NiO and Cu-doped NiO nanostructures. It was observed that the decrease in the size of particles and increase the band gap occur with increase in Cu doping concentration. The optical band gap of NiO and Cu-doped NiO nanoparticles can be tuned from 3.80 to 4 eV with the increase of Cu doping concentration. The crystal size of samples was found 49–55 nm at the different temperatures and was calculated as 47-49 nm. The study on the magnetic property of the samples using VSM technique shows that the Cu-doped NiO nanoparticles behaves as a super-paramagnetic material.

References

1. R. Paulose, R. Mohan, V. Parihar, *NANOSO*, 11, **2017**, 102.
2. A. Akbari, M. Amini, A. Tarassoli, B. Eftekhari-Sis, N. Ghasemian, E. Jabbari, *NANOSO*, 14, **2018**, 19.
3. G. Ma, S. Salahub, C. Montemagno, S. Abraham, *NANOSO*, 13, 2018, 74.
4. Y. X. Li, K. J. Klabunde, *Langmuir*, 7, **1991**, 1388.
5. N. Sekine, C-H. Chou, W. L. Kwan, Y. Yang, *Org Electron*, 10, **2009**, 1473.
6. H. J. Kwon, K. Shin, M. Soh, H. Chang, J. Kim, J. Lee, et al., *Adv. Mater.*, **2018**, 1704290.
7. S. M. Abdelbasir, S. M. El-Sheikh, M. M. Rashad, D. A. Rayan, *Electron. Mater. Lett.*, 14, **2018**, 505.
8. B. Hillary, P. Sudarsanam, M. H. Amin, S. K. Bhargava, *Langmuir*, 33, **2017**, 1743.
9. J. W. Jung, C. Chueh, A. K. Jen, *Adv. Mater.*, 27, **2015**, 7874.
10. P. Ponnusamy, S. Agilan, N. Muthukumarasamy, *Int. J. Chem. Sci.*, 13, **2015**, 683.
11. K-C., Wang, J-Y. Jeng, P-S. Shen, Y-C. Chang, E. W-G. Diau, C-H. Tsai, et al., *Sci. Rep.*, 4, **2014**, 4756.
12. J. Huang, N. Zhu, T. Yang, T. Zhang, P. Wu, Z. Dang, *Biosens. Bioelectron.*, 72, **2015**, 332.
13. Z. Wang, L. Xing, J. Li, M. Xu, W. Li, *J. Power. Sources.*, 307, **2016**, 587.
14. J. A. Dirksen, K. Duval, T. A. Ring, *Sensor. Actuat. B-Chem.*, 80, **2001**, 106.
15. M-S. Wu, Y-A. Huang, C-H. Yang, J-J. Jow, *Int. J. Hydrogen. Energ.* 32, **2007**, 4153.
16. B. Sasi, K. G. Gopchandran, *Nanotechnology.*, 18, **2007**, 115613.
17. F. Tietz, F. J. Dias, D. Simwonis, D. Stöver, *J. Eur. Ceram. Soc.*, 20, **2000**, 1023.
18. G. A. Niklasson, C. G. Granqvist, *J. Mater. Chem.*, 17, **2007**, 127.
19. V. Srinivasan, J. W. Weidner, *J. Electrochem. Soc.*, 144, **1997**, L210.
20. X. Zhu, H. Dai, J. Hu, L. Ding, L. Jiang, *J. Power. Sources.*, 203, **2012**, 243.
21. P. Matteazzi, G. L. Caër, *J. Am. Ceram. Soc.*, 75, **1992**, 2749.
22. A. C. Sonavane, A. I. Inamdar, P. S. Shinde, H. P. Deshmukh, R. S. Patil, P. S. Patil, *J. Alloys. Compd.*, 489, **2010**, 667.
23. Y. F. Yuan, X. H. Xia, J. B. Wu, Y. B. Chen, J. L. Yang, S. Y. Guo., *Electrochim. Acta.*, 56, **2011**, 1208.
24. X. Jiang, Y. Wang, T. Herricks, Y. Xia, *J. Mater. Chem.*, 14, **2004**, 695.
25. T. K. Sau, A. L.Rogach, *Adv. Mater.*, 22, **2010**, 1781.
26. H. Cui, Y. Feng, W. Ren, T. Zeng, H. Lv, Y. Pan, *Rec. Pat. Nanotech.*, 3, **2009**, 32.
27. N. Saito, H. Haneda, T. Sekiguchi, N. Ohashi, I. Sakaguchi, K. Koumoto, *Adv. Mater.*, 14, **2002**, 418.

28. P. R. Patil, V. E. Krishnamurthy, S. S. Joshi, *Propellants. Explos. Pyrot.,* 33, **2008**, 266.
29. S. Kumar, Y. J. Kim, B. H. Koo, J. Lee, *Nanosci. Nanotechnol.*, 10, **2010**, 7204.
30. J. Tauc, Optical properties of solids, Academic Press Inc, (1966), New York, USA.
31. A. Sharma, S. Pallavi, S. Dahiya, N. Budhiraja, *Adv. App. Sci. Res.*, 4, **2013**, 124.
32. F. Davar, Z. Fereshteh, M. Salavati-Niasari, *J. Alloy. Compd.*, 476, **2009**, 797.
33. A. Rahdar, M. Aliahmad, Y. Azizi, *J. Nanostructures*., 5, 2015, 145.
34. K. Borgohain, J. Singh, B. Rao, M. R. Shripathi, S. Mahamuni, *Phys. Rev. B.*, 61, **2000**, 11093.
35. A. Wang, H. Yin, M. Ren, H. Lu, J. Xue, T. Jiang, *New. J. Chem.*, 34, **2010**, 708.
36. K. Sathishkumar, N. Shanmugam, N. Kannadasan, S. Cholan, G. Viruthagiri, *J. Sol-Gel Sci.Tech.*, 74, **2015**, 621-630.